Hindawi
Journal of Sensors
Volume 2021, Article ID 5564932, 9 pages
https://doi.org/10.1155/2021/5564932

Research Article

The Analysis and Simulation with the Fatigue Life of Hemispherical Resonator Gyro

Lijun Song,[1] **Jiayao Ni**,[1] **Lei Zhou**,[1] **Wangliang Zhao**,[2] **Shaoliang Li**,[2] **and Minghui Lu**[1]

[1]*Xi'an University of Architecture and Technology, School of Information and Control Engineering, Xi'an, Shaanxi 710055, China*
[2]*Shanghai Institute of Aerospace Control Technology, Shanghai 201109, China*

Correspondence should be addressed to Lijun Song; songlijun9071@sina.com

Received 10 February 2021; Revised 23 April 2021; Accepted 14 May 2021; Published 2 June 2021

Academic Editor: Li Shuai

The life and damage of hemispherical resonator are important factors that directly affect the service time and safety of high-precision hemispherical resonator gyro. However, the fused silica glass material used in the hemispherical resonator which was processed in China is mainly imported, and it is too expensive to use the traditional fatigue life experiment, so it is necessary to use the software of fatigue life analysis to analyze its fatigue life. In the paper, the ANSYS software is used to analyze the fatigue life of fused silica hemispherical resonator, to determine the dangerous parts caused by the residual stress to analyze the crack propagation in the fatigue parts, and to obtain the sum stress intensity factor, so as to effectively monitor and prevent the fatigue-prone parts in the process of structural design and use of the hemispherical resonator.

1. Introduction

Hemispherical resonator gyroscope (HRG) has been widely used and paid attention to in the field of inertial technology at home and abroad due to the performance optimization of HRG [1]. The isotropic material is the basis of HRG with high quality, and the HRG with high-precision spherical shell structure is the core technology [2].

At present, the ideal material of hemispherical resonator is fused silica glass [3]. According to the research and development of the fused silica glass in China, as well as the research results and experience of hemispherical resonator processing technology at home and abroad, combined with the technical bottleneck of fused silica glass in ultraprecision machining of complex curved surface, it is necessary to consider the resonator processing technology, resonator quality factor test, frequency difference test, material uniformity, and coating technology as a system engineering to study [4].

2. The Basic Structure of Hemispherical Resonator

The core component of HRG is hemispherical resonator which was made of fused silica glass. The basic shape is a thin-walled hemispherical shell fixed by a cylindrical support rod in the pole area, and it is hemispherical elastomeric, which makes the bending energy storage of each gram of resonator material reach the maximum value [5]. The support rod is integrated with the hemispherical shell. On the one hand, the support rod can restrain and support the harmonic resonator; on the other hand, it can also transfer electric signals. The common diameter of the support rod is 15~60 mm, and the wall thickness is 0.3~1 mm. The structure of the hemispherical resonator is shown as Figure 1.

$R = 15$ mm is the midplane radius of the hemispherical resonator; $h = 1$ mm is the wall thickness of the hemispherical resonator; $r = 3$ mm is the radius of the support rod; $L_1 = 5$ mm, $L_2 = 10$ mm, and $L = 30$ mm are the lengths of

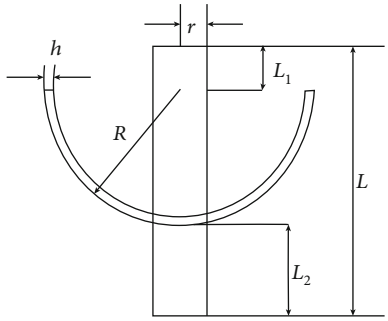

Figure 1: The structure diagram of the hemispherical resonator.

the support rod at different positions. The material of hemispherical resonator is fused silica glass.

In order to analyze the dynamic performance of HRG, Solid Works software is used to draw the two-dimensional sketch of the hemispherical resonator with single end constraint, and then, the three-dimensional hemispherical resonator model is obtained by rotation degree [6]. The solid-45 element of 8 nodes is selected to grid hemispherical resonator with a mapping method, and each finite element of the hemispherical resonator is an 8-node hexahedral element, where Young's modulus of the fused silica glass is $E = 76700\ Mpa$, the density is $2.2 \times 10^3\ kg/m^3$, and Poisson's ratio is 0.17.

3. The Stress Analysis of Hemispherical Resonator

3.1. The Stress Intensity Factor. Stress intensity factor (SIF) is a key parameter to drive the crack growth, which represents the crack growth rate of the hemispherical resonator and reflects the stress intensity near the crack tip [7, 8]. The relationship between the stress intensity factor and the microstress σ at the surface crack tip of the hemispherical resonator is as follows:

$$K = Y \cdot \sigma \sqrt{\pi a}. \tag{1}$$

Y is the dimensionless coefficient of the geometry of the hemispherical resonator.

There are different stress intensity factors for different crack growth types, which are open mode (type I), sliding mode (type II), and tearing mode (type III) [9].

Type I is caused by the low stress fracture. The plane of crack generation is perpendicular to the displacement direction of the crack surface, and the two crack surfaces open and separate. The calculation of stress in each direction is shown in the following equation:

$$\begin{aligned} \sigma_x &= \frac{K_{\mathrm{I}}}{\sqrt{2\pi r}} \cos\frac{\theta}{2}\left(1 - \sin\frac{\theta}{2}\sin\frac{3\theta}{2}\right), \\ \sigma_y &= \frac{K_{\mathrm{I}}}{\sqrt{2\pi r}} \cos\frac{\theta}{2}\left(1 + \sin\frac{\theta}{2}\sin\frac{3\theta}{2}\right), \\ \sigma_z &= 0. \end{aligned} \tag{2}$$

Type II is caused by the sliding of the upper and lower surfaces due to the shear stress parallel to the crack plane. The calculation of stress in each direction is shown in the following equation:

$$\begin{aligned} \sigma_x &= \frac{-K_{\mathrm{II}}}{\sqrt{2\pi r}} \sin\frac{\theta}{2}\left(2 + \cos\frac{3\theta}{2}\cos\frac{3\theta}{2}\right), \\ \sigma_y &= \frac{K_{\mathrm{II}}}{\sqrt{2\pi r}} \sin\frac{\theta}{2}\cos\frac{\theta}{2}\cos\frac{3\theta}{2}, \\ \sigma_z &= 0. \end{aligned} \tag{3}$$

Type III is staggered of the upper and lower surfaces due to the shear stress parallel to the crack surface and the crack front; the calculation of stress in each direction is shown in the following equation:

$$\begin{aligned} \tau_{xz} &= -\frac{K_{\mathrm{II\ I}}}{\sqrt{2\pi r}} \sin\frac{\theta}{2}, \\ \tau_{zy} &= -\frac{K_{\mathrm{III}}}{\sqrt{2\pi r}} \cos\frac{\theta}{2}, \\ \sigma_x &= \sigma_y = \sigma_z = \tau_{xy} = 0. \end{aligned} \tag{4}$$

3.2. The Analysis of Residual Stress. The equivalent stress follows the fourth strength theory of material mechanics [10]. Stress isoclines are used to represent the stress distribution inside the model, and the results in the whole model are clearly described, so that the most dangerous areas in the model can be quickly identified. Stress alternation is an important cause of material fatigue, and the frequency of stress alternation also has a direct effect on the fatigue of hemispherical harmonic oscillator.

The residual stress is the internal stress of self balance in the component, which is the stress in the component to achieve balance when there is no external factor [11]. It is mainly caused by the nonuniformity of internal plastic deformation in the process of component, and its magnitude is related to the plastic deformation of component material [12]. In the process of blank preparation, mechanical processing, heat effect treatment, and electronic assembly, residual stress will be produced [13]. The residual stress is generally harmful; sometimes, it will not immediately appear as a defect, but when the total stress which is superposed of working stress and residual stress exceeds the strength limit, it will cause sudden damage, which will seriously affect the size of the component stability, machining accuracy, and static strength. The residual stress also has beneficial aspects, which can improve the fatigue strength and wear resistance of the hemispherical resonator by appropriate controls [14].

3.3. The Simulation with Stress Analysis of Hemispherical Resonator

3.3.1. Preprocessing of Simulation. The model of the hemispherical resonator is drawn by Solid Works and imported it into ANSYS; the paper defined the parameters of fused silica glass and then divided the grid of the hemispherical resonator as shown in Figure 2:

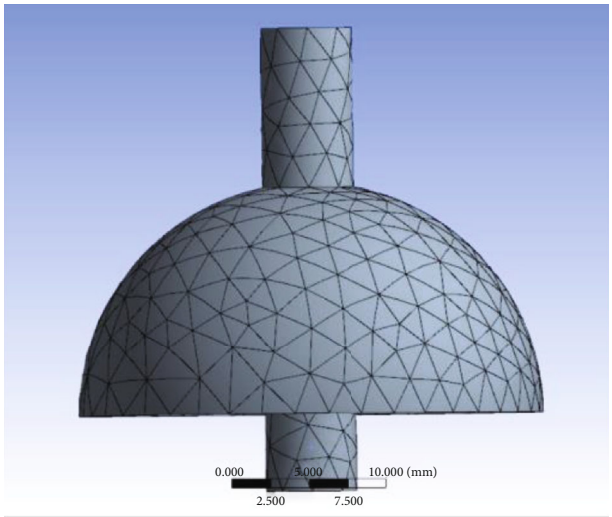

Figure 2: The grid finite element model of the hemispherical resonator.

3.3.2. Simulation of Stress Change. In the paper, all the degrees of freedom of the upper end of the support rod are limited, the hemispherical shell and the following parts are free, and the structural static analysis of the hemispherical resonator is carried out in ANSYS. The stress variation of the hemispherical resonator is analyzed by applying a pressure of 0.5 MPa on the hemispherical spherical surface and a tension in the direction perpendicular to the spherical surface. The constrained diagram model of the hemispherical resonator is shown in Figure 3.

3.3.3. Postprocessing of Simulation. After defining the materials, applying loads and constraints, and adding results, the model is ready to be solved. Once the solution is completed, the solution results can be viewed and the postprocessing solution results are as follows.

According to the simulation diagram of the equivalent stress of residual stress (Figure 4), the maximum value of equivalent stress is 569.43 MPa at the fixed constraint end, and the minimum value of equivalent stress is 1.6795*e*-5 MPa.

According to the simulation of residual stress intensity (Figure 5), the maximum value of residual stress intensity is 576.62 MPa at the fixed constraint end, and the minimum value of equivalent stress is 1.9098*e*-5 MPa.

4. The Analysis of Crack Propagation and Fatigue Life

4.1. The Fatigue Life of Hemispherical Resonator. Fatigue life is the number of cycles experienced by the hemispherical resonator when fatigue damage occurs under stress or the duration of time subjected to stress. The fatigue life is mainly affected by the size of the material, the concentration of the loading stress, the surface finish of the material specimen, and the frequency of the type of loading load [15].

The traditional method of fatigue life determination is based on fatigue damage theory and a large number of life test data. The fatigue data of the hemispherical resonator are obtained by using the same or similar experiments with the actual situation of the component [16]. Then, the fatigue life of different schemes is analyzed by using the fatigue life to check whether the fatigue life of the hemispherical resonator component meets the design requirements, and the fatigue life prediction model and method are established and carried out scientific processing in the process of component processing to effectively improve the fatigue strength of materials [17].

4.2. The Analysis of Crack Propagation. In practical engineering applications, fatigue crack propagation is also an important part of fatigue life prediction. The fatigue propagation is caused by the cyclic alternating load. The fatigue propagation is generated from the surface, and it will propagate along the direction perpendicular to the main stress of the crack. The crack propagation accelerates, and the stress increases gradually [18]. When it reaches the limit of the stress intensity of the material, the ultimate instantaneous fracture will occur.

The coordinate system of three-dimensional crack and tip in the hemispherical resonator can be abstracted as shown in Figure 6.

According to the mechanical analysis of the surface cracks by linear elastic fracture mechanics, the relationship between the displacement field near the crack tip generated by any accidental load and the stress intensity factor can be expressed as follows:

$$\begin{bmatrix} u \\ v \\ w \end{bmatrix} = \frac{K_{\mathrm{I}}}{4G}\sqrt{\frac{r}{2\pi}}\begin{bmatrix} (2k-1)\cos\dfrac{\theta}{2} - \cos\dfrac{3\theta}{2} \\ (2k+1)\sin\dfrac{\theta}{2} - \sin\dfrac{3\theta}{2} \\ 0 \end{bmatrix} + \frac{K_{\mathrm{II}}}{4G}\sqrt{\frac{r}{2\pi}}\cdot\begin{bmatrix} (2k+3)\sin\dfrac{\theta}{2} + \sin\dfrac{3\theta}{2} \\ (3-2k)\cos\dfrac{\theta}{2} - \cos\dfrac{3\theta}{2} \\ 0 \end{bmatrix} + \frac{K_{\mathrm{III}}}{4G}\sqrt{\frac{r}{2\pi}}\begin{bmatrix} 0 \\ 0 \\ 8\sin\dfrac{\theta}{2} \end{bmatrix}, \tag{5}$$

where r is the crack propagation length; θ is the crack cracking angle; and K_{I}, K_{II}, and K_{III} are stress intensity factors of different types. u, v, and w are the radial displacement, normal displacement, and tangential displacement of the crack tip. G is the shear modulus; K is the constant related to the material.

If the displacement of a point between the upper and lower crack surface is known, the crack stress intensity factor can be obtained as follows:

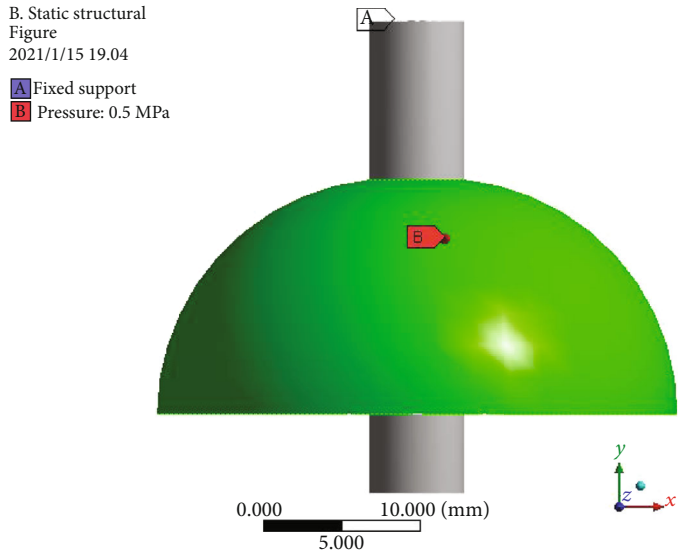

Figure 3: The constrained diagram model of the hemispherical resonator.

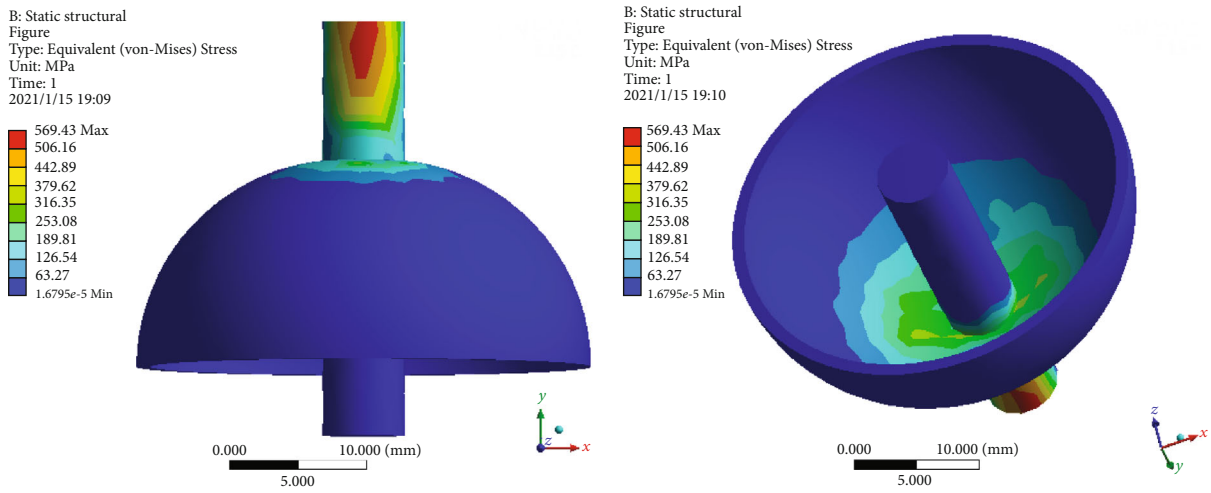

Figure 4: Simulation of the equivalent stress of residual stress.

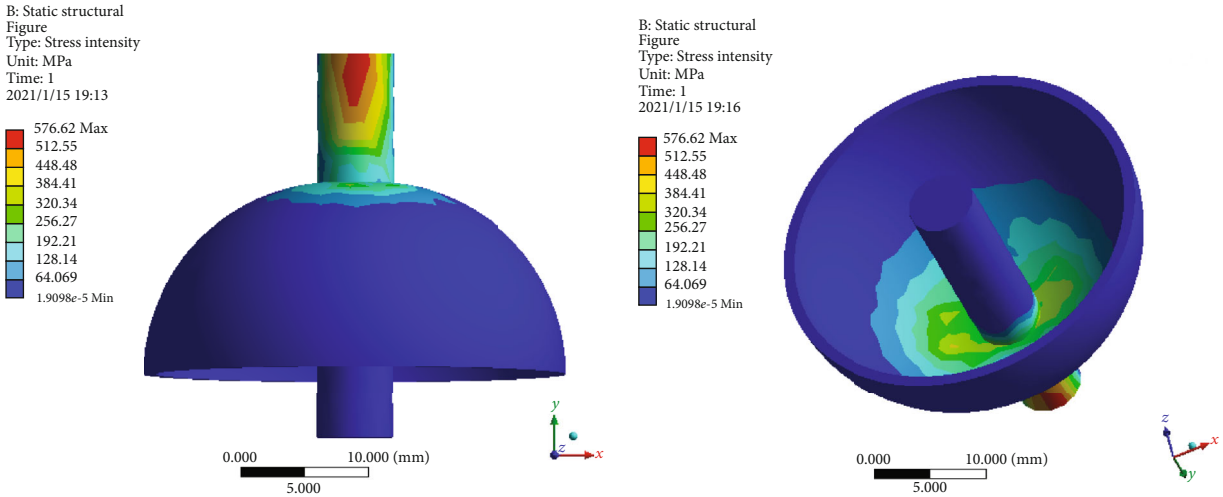

Figure 5: Simulation of residual stress intensity.

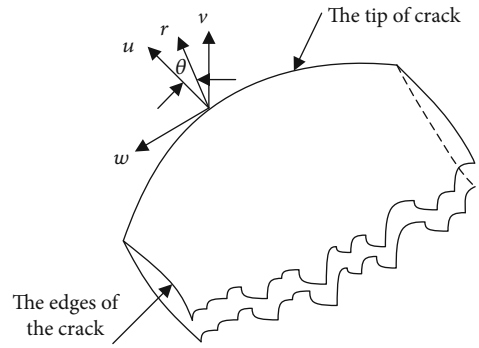

Figure 6: The coordinate system of the crack tip.

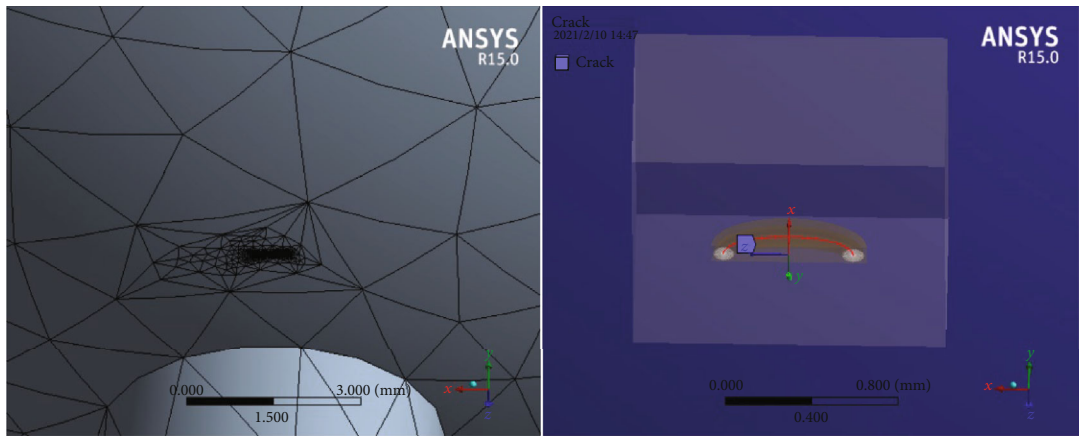

Figure 7: The elliptical surface crack.

$$\begin{bmatrix} K_{\mathrm{I}} \\ K_{\mathrm{II}} \\ K_{\mathrm{III}} \end{bmatrix} = \lim_{r \longrightarrow 0} \frac{2G}{k+1} \sqrt{\frac{2\pi}{r}} \begin{bmatrix} v \\ u \\ (k+1)\dfrac{w}{4} \end{bmatrix}_{\theta=\pm\pi}. \quad (6)$$

In this paper, the model-based finite element method is used to analyze the stress intensity factor of HRG subsurface crack under residual stress state, which provides the theoretical basis for the fatigue life prediction of HRG.

According to the elliptical surface crack (Figure 7), the main radius of the crack is 0.3 mm and the secondary radius is 0.1 mm. The X-axis is the direction of crack propagation, the Y-axis is the normal direction of crack propagation, and the Z-axis is the dominant direction of elliptical crack. After loading, the equivalent stress deprogram and stress-intensity factor diagrams of type I, IIs and III fractures are shown in Figures 8 and 9.

It can be seen from Figure 8 that there is a small stress change at the connection between the support rod and the hemispherical shell. According to Figure 9, the stress intensity factor of type I $K_{\mathrm{I}} = 0.13932\, Mpa \cdot mm^{1/2}$, type II $K_{\mathrm{II}} = -33.446\, Mpa \cdot mm^{1/2}$, and type III $K_{\mathrm{III}} = -12.098\, Mpa \cdot mm^{1/2}$ was calculated by ANSYS.

4.3. The Fatigue Life Analysis of HRG

4.3.1. The Miner Theory. It is assumed that the stress reaching the fatigue stress limit will not damage the hemispherical resonator components, and the loading sequence of the variable amplitude stress load has no effect on the accumulated fatigue damage. According to Miner's theory,

(1) when the component is subjected to constant amplitude load, the damage of the component caused by one cycle is

$$D = \frac{1}{N}, \quad (7)$$

where N is the fatigue life corresponding to the current load level

The damage caused by N cycles is as follows:

$$D = \frac{n}{N}. \quad (8)$$

At that $n = N$, fatigue failure occurred.

(2) The component is subjected to variable amplitude loads of different stress levels $\Delta\sigma_i$ and undergo several n_i cycles under the action of stress levels. The damage caused by per cycle is $1/N_i$, and then, the fatigue damage of each n_i cycle is $D_i = n_i/N_i$. When fatigue damage occurs after damage accumulation,

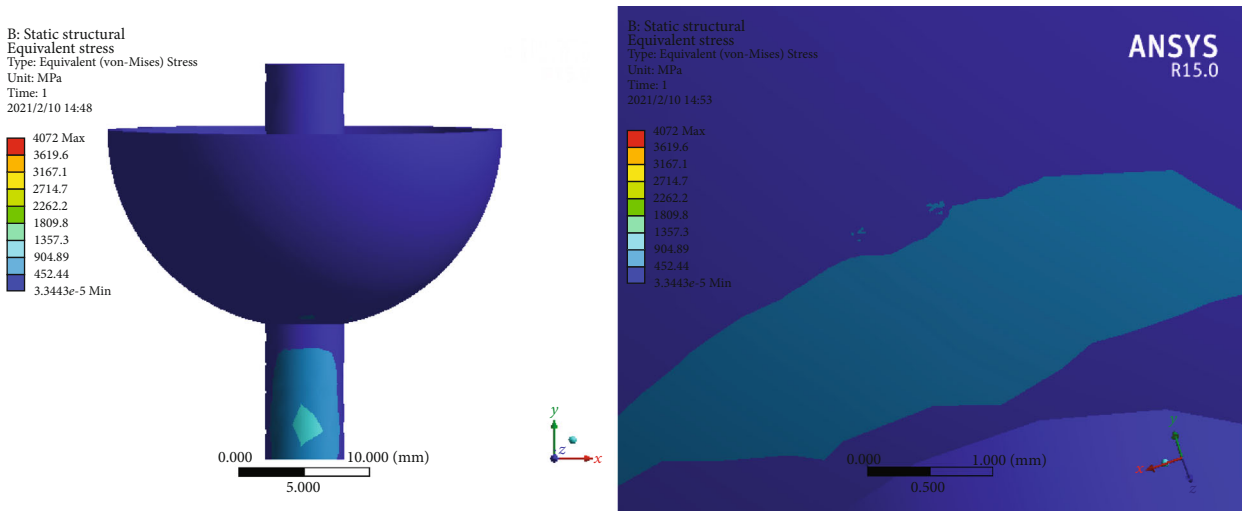

Figure 8: Overall and local stress nephogram.

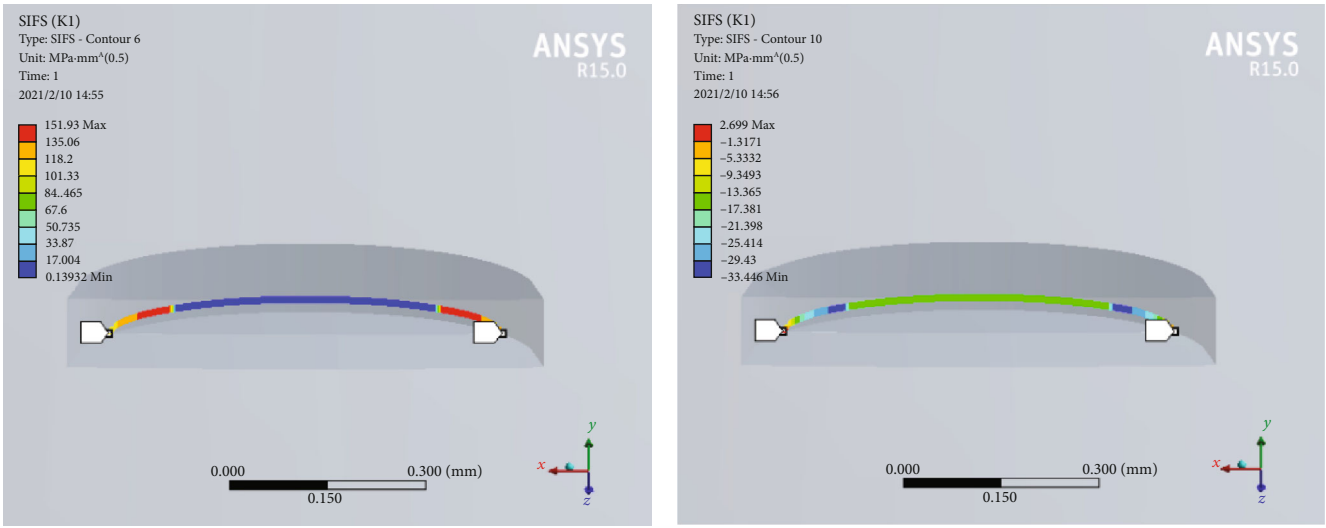

(a) K_I cloud map

(b) K_{II} cloud map

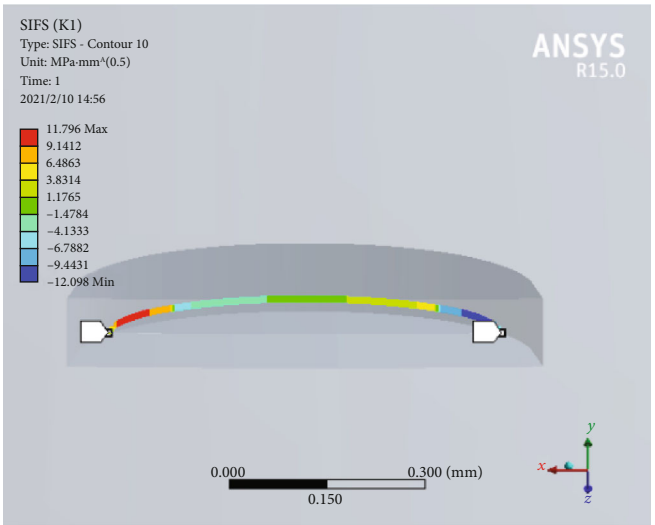

(c) K_{III} cloud map

Figure 9: The stress-intensity factor diagrams.

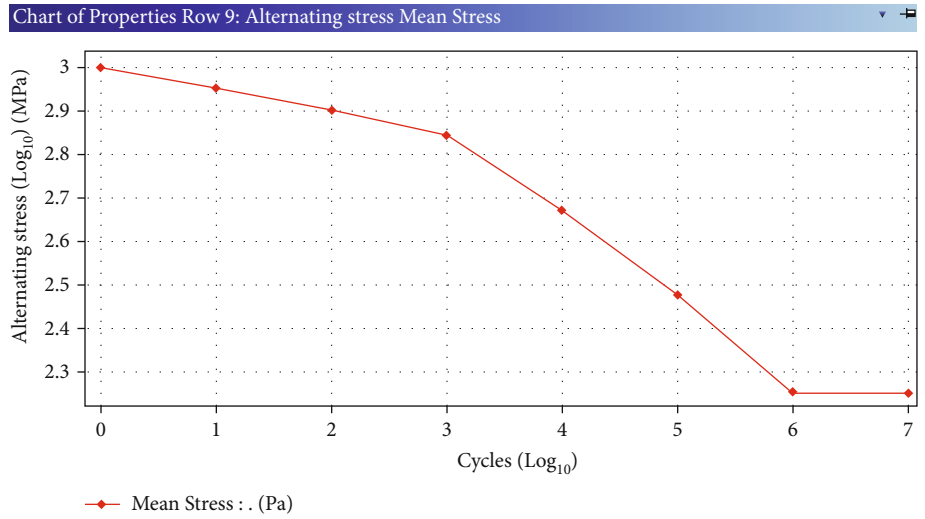

Figure 10: *S-N* curve.

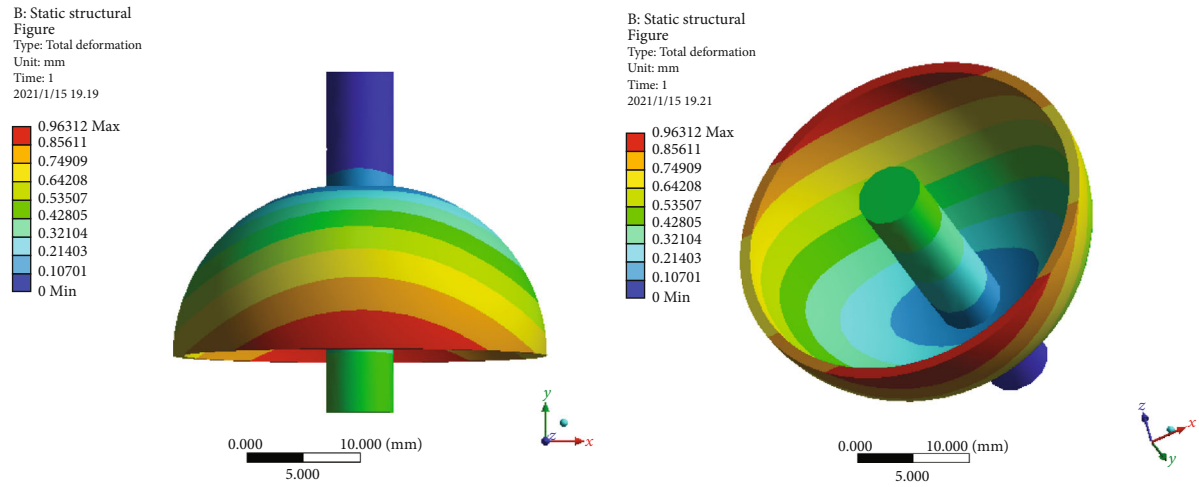

Figure 11: Deformation simulation diagram.

$$D = \sum_{i=1}^{k} D_i = \sum_{i=1}^{k} \frac{n_i}{N_i} = 1, \tag{9}$$

where N_i is the number of cycles corresponding to stress level $\Delta\sigma_i$ on the *S-N* curve

4.3.2. Fatigue Resistance Curve. The fatigue life prediction method of HRG is based on the *S-N* (stress cycle-number) curve to estimate the life, and the total life can be obtained directly. At present, in fatigue life prediction engineering, Basquin formula is commonly used to express the relationship between fatigue life and stress under constant amplitude load. The expression is as follows:

$$\sigma_a = \sigma_f'(2N_f)^b = \frac{E\Delta\varepsilon_e}{2}, \tag{10}$$

where N_f is the number of fatigue life cycles until the component is destroyed; σ_a is the stress amplitude; and σ_f' is the fatigue strength coefficient of the component, in which σ_f' is consistent with the real stress coefficient σ_f under static tensile fracture. b is the fatigue strength index.

The power function expression of the corresponding *S-N* curve can be obtained from the above equation as follows:

$$\sigma^m N = C, \tag{11}$$

where N is the number of fatigue life cycles and m and C are the parameters related to material properties and loads.

During the normal operation of gyro, the position where HRG is most prone to fatigue failure is the fixed constraint end of the rod. Based on the results of finite element analysis, MSC fatigue analysis and design tool are used to calculate the stress value of the hemispherical resonator, and the *S-N* curve is interpolated with the stress value to obtain the fatigue life of the hemispherical resonator. The *S-N* curve is shown in Figure 10.

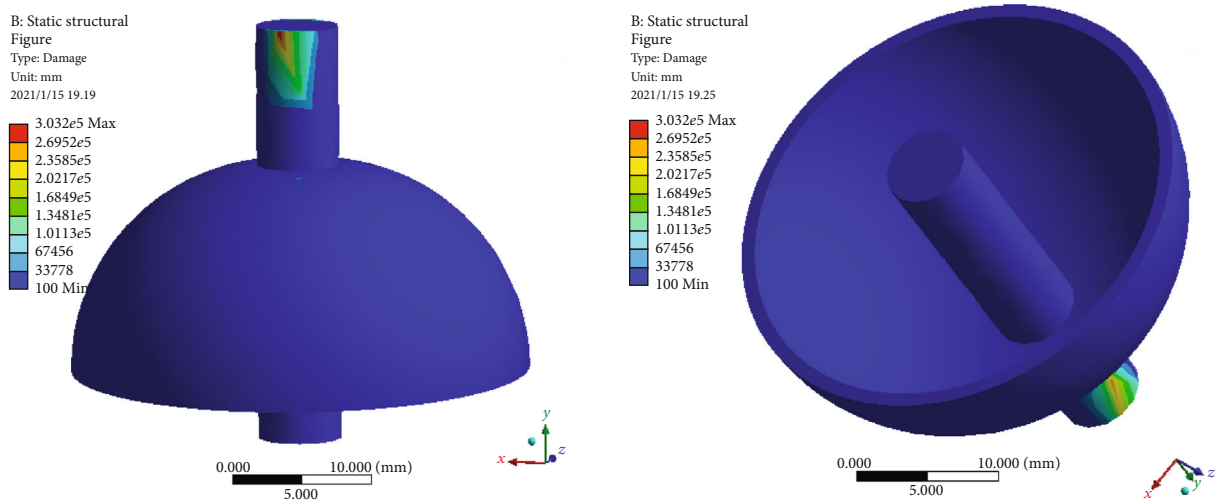

Figure 12: Damage simulation diagram.

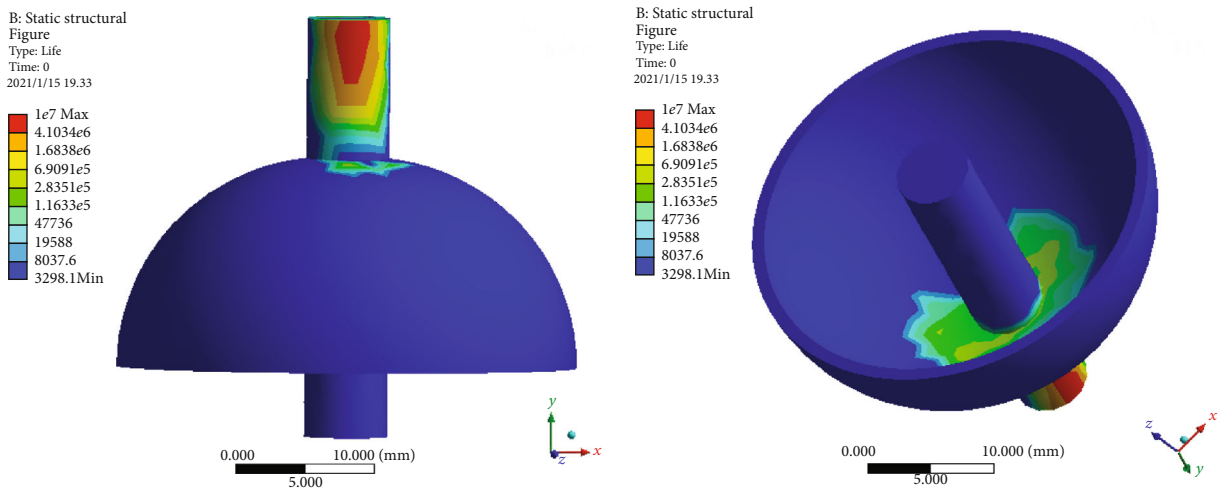

Figure 13: Fatigue life simulation diagram.

The *S-N* curve is the relationship between alternating stress and fracture cycles of the material, which is generally obtained by experiments. The logarithm of the stress intensity of the standard specimen of fused silica material is taken as the ordinate, and the logarithm of the fatigue life is taken as the abscissa to represent the relationship between the fatigue strength and the fatigue life of the standard sample under certain cyclic characteristics.

4.3.3. The Simulation of Fatigue Life. Miner cumulative fatigue criterion is used for fatigue calculation. Under the hypothesis of this theory, deformation simulation, damage simulation, and safety factor simulation are shown in Figures 11–13.

According to the cloud image analysis, there is almost no deformation in the constraint end of the model, while there are different degrees of deformation in other parts of the model, with the maximum value up to 0.96312 mm.

According to the cloud image analysis, the existence of 0.5 MPa residual stress would cause different degrees of damage to different parts of the model, and the maximum value can reach 3.032*E*5. In addition, there is slight damage near the contact surface between the ball and the rod, ranging from 33778 to 67456.

The results of fatigue life solution are shown in Figure 13.

According to the analysis of fatigue life simulation diagram, under the action of residual stress, the position with the shortest life is the red area in the figure, and the life cycles in this area is 3298.1. The blue area has the longest life, and the life cycle is 1*e*7 times, which indicates that the blue area can work indefinitely in the presence of residual stress.

5. Conclusion

The most common failure mode of failure is the fatigue damage. In this paper, ANSYS software is used to simulate

the effect of residual stress on the damage and crack propagation of the fused silica hemispherical resonator. The maximum residual stress of the hemispherical resonator is 569.43 MPa. Due to the existence of residual stresses, the hemispherical resonators will produce different degrees of deformation and damage in the parts outside the constraint area. The Miner cumulative fatigue criterion is used for the end fatigue calculation. The shortest life is 3298.1 times, and the longest life cycle is 1*e*7 times. The fatigue hazard area caused by residual stress is determined as the fixed restrained end of the hemispherical resonator rod, and the crack propagation analysis is performed at the fatigue area, and three crack stress intensity factors $K_{\mathrm{I}} = 77.656\,Mpa \cdot mm^{1/2}$, $K_{\mathrm{II}} = -272.34\,Mpa \cdot mm^{1/2}$, and $K_{\mathrm{III}} = -23.82\,Mpa \cdot mm^{1/2}$ are obtained, which provide theoretical support for structural design and engineering applications of hemispherical resonators.

Data Availability

The raw/processed data required to reproduce these findings cannot be shared at this time as the data also forms part of an ongoing study.

Conflicts of Interest

We declare that we do not have any commercial or associative interest that represents a conflict of interest in connection with the work submitted.

Acknowledgments

This work is partially supported by the Natural Science Foundation of Shaanxi Province, the project number 2020JM-488, and the special scientific research project of the Education Department of Shaanxi Province, the project number 20JK0728.

References

[1] S. Yang and M. Liu, "Analysis of the crack penetration/deflection at the interfaces in the intelligent coating system utilizing virtual crack closure technique," *Engineering Fracture Mechanics*, vol. 133, pp. 152–162, 2015.

[2] Y. Pan, Q. Tianliang, K. Yang, and H. Luo, "Research status and development trend of hemispherical resonator gyroscope," *Navigation, Positioning and Timing*, vol. 4, no. 2, pp. 9–13, 2017.

[3] L. Xue, Y. Shen, S. Lijun, and C. Xiaozhen, "Overview of foreign navigation technology development in 2019," *Navigation and Control*, vol. 19, no. 2, pp. 1–9, 2020.

[4] P. Hui, T. W. Guo, F. Haibin, and Y. Longhui, "Technical characteristics of development of hemispherical resonator gyroNavigation," *Positioning and Timing*, vol. 6, no. 4, pp. 108–114, 2019.

[5] W. Zhao, H. Yang, W. Wang, S. Li, Y. Cheng, and L. Song, "Research on full angle mode control technology of hemispherical resonator gyro," *Navigation, Positioning and Timing*, vol. 6, no. 6, pp. 8–13, 2019.

[6] S. Lijun, Z. Lei, L. Shaoliang, and F. Qiangwen, "Research on precession characteristics of circumferential mode of hemispherical gyro resonator," *Navigation, Positioning and Timing*, vol. 6, no. 6, pp. 19–26, 2019.

[7] L. Xiaoxing and C. Wenming, "Fatigue causes analysis of metal parts and measures to improve fatigue strength," *China Metal Bulletin*, vol. 11, pp. 179-180, 2018.

[8] C. X.-d. Morning and W. Wujing, "I II - III compound crack stress intensity factors and energy release rate," *Journal of Hebei University of Engineering (Natural Science Edition)*, vol. 33, no. 4, pp. 10–13, 2016.

[9] Z. Shaoqing and S. Guo, "Research on stress field at crack tip of concrete," *Journal of Wuhan University of Technology*, vol. 33, no. 10, pp. 78–82, 2011.

[10] L. Jingxiu, S. Wei, X. Yang, L. Guofu, and J. Jibin, "Stress intensity factor analysis of TBM cutterhead crack under complex stress state," *Journal of Harbin Engineering University*, vol. 38, no. 4, pp. 633–639, 2017.

[11] Q. Zhen, Z. Guo, H. Wang, and Z. Pengxiang, "Fatigue strength analysis of cargo bogie based on finite element method," *Railway Technical Supervision*, vol. 48, no. 7, pp. 35–39, 2020.

[12] H. Kang and R. Yang, "Fatigue analysis of vehicle lateral stabilizer rod based on ANSYS," *Journal of Machine Design*, vol. 25, no. 12, pp. 66–68, 2008.

[13] Y. Wang, J. Luo, Y. Jun, and C. Liping, "Fatigue analysis method and practice based on finite element," *Machinery Design & Manufacture*, vol. 1, pp. 22–24, 2008.

[14] J. Liu, H. Zhang, and J. Li, "I based on extended finite element method (FEM) - II complex crack extension study," *Journal of Beijing Institute of Technology*, vol. 9, pp. 881–885, 2015.

[15] L.-J. Song, R. Yang, W.-L. Zhao, X. He, S. Li, and Y.-J. Ding, "Research on the precession characteristics of hemispherical resonator gyro," *Complexity*, vol. 2021, Article ID 8825017, 9 pages, 2021.

[16] D. M. Rozelle, "The hemispherical resonator gyro: from wineglass to the planets," in *Proceedings of 19th AAS/AIAA Space Flight Mechanics Meeting*, vol. 134, pp. 1–26, Savannah, GA, USA, 2009.

[17] Q. Zeng, Y. Li, J. Shi et al., "Fatigue life analysis of supercharged boiler based on the design by analysis method," *International Journal of Pressure Vessels and Piping*, vol. 188, article 104217, 2020.

[18] V. E. Dzhashitov and V. M. Pankratov, "Mathematical models of the thermoelastic stress–strain state, temperature, and technological errors of a wave solid-state sensor of inertial informations of inertial information," *Journal of Machinery Manufacture and Reliability*, vol. 39, no. 3, pp. 248–255, 2010.